

Geochemical characterisation of the Ellsworth-Whitmore Mountains crustal block: a critical piece in the puzzle to unravel ice retreat in West Antarctica

Emily J. Archibald^{a,*}, James W. Marschalek^a, Adrian R. Muxworthy^a, Teal R. Riley^b, Claus-Dieter Hillenbrand^b, Tom A. Jordan^b, Pieter Vermeesch^c, Michael J. Flowerdew^d, Martin Siegert^{a,e}, Dominic A. Hodgson^b, Tina van de Flierdt^a

^a Department of Earth Science and Engineering, Imperial College London, London, UK

^b British Antarctic Survey, Cambridge, UK

^c Department of Earth Sciences, University College London, London, UK

^d CASP, Cambridge, UK

^e Tremough House, University of Exeter, Penryn, Cornwall, UK

ARTICLE INFO

Editor: Don Porcelli

Keywords:

West Antarctic Ice Sheet
Sediment provenance
Geochemistry
Neodymium and strontium isotopes
Zircon U-Pb

ABSTRACT

The West Antarctic Ice Sheet (WAIS) is prone to major retreat. Identifying when previous WAIS retreats occurred could improve sea level rise projections, but detection of these events in marine sediments is limited by knowledge of the geochemical signature of key sediment source regions located further inland - primarily the Ellsworth-Whitmore Mountains (EWM). This is because a smaller WAIS would likely result in enhanced erosion of the EWM and permit more widespread transport of EWM detritus offshore. We here characterise the provenance signature of the EWM, showing that different stratigraphic units exhibit distinct geochemical characteristics based on unique combinations of zircon U-Pb ages and Nd and Sr isotope ratios. The oldest Heritage Group displays dominant Grenville Orogeny (1000–1250 Ma) ages, with mean ϵ_{Nd} values of ~ -8 and $^{87}Sr/^{86}Sr$ ratios of ~ 0.719 . The overlying Crashsite Group and Whiteout Conglomerate exhibit dominant Ross Orogeny ages (490–580 Ma), with mean ϵ_{Nd} values of ~ -12 and -18 and $^{87}Sr/^{86}Sr$ ratios of ~ 0.740 and ~ 0.725 , respectively. The youngest Polarstar Formation has common Permian zircon U-Pb ages and ϵ_{Nd} values of ~ -4 and $^{87}Sr/^{86}Sr$ ratios of ~ 0.711 . Outlying nunataks are assigned to the Heritage and Crashsite groups, extending our geological knowledge of the Ellsworth Subglacial Highlands. Together, our data suggest that the Ellsworth Mountains crustal block is characterised by a mean ϵ_{Nd} value of ~ -10 , $^{87}Sr/^{86}Sr$ ratio of ~ 0.728 , and bimodal Ross and Grenville orogeny zircon U-Pb ages. This “provenance fingerprint” should be identifiable in offshore sediments recording times of major WAIS retreat.

1. Introduction

If the West Antarctic Ice Sheet (WAIS) was to be lost completely, it would raise global mean sea level by ~ 5.3 m (Morlighem et al., 2020). Satellite observations have documented significant WAIS deglaciation over recent decades (Rignot et al., 2019; Smith et al., 2020), questioning the long-term stability of the ice sheet. With approximately 75% of the WAIS grounded below sea level (Church et al., 2013) and its bed dipping towards the West Antarctic interior in several drainage sectors (e.g., Ross et al., 2012; Pritchard et al., 2025), it is particularly vulnerable to incursions of warm ocean water and marine ice sheet instability (Joughin et al., 2014; Hillenbrand et al., 2017). The present day ocean

forcing may be sufficient to trigger significant and irreversible (on human timescales) deglaciation of West Antarctica in the coming centuries (Joughin et al., 2014; Favier et al., 2014; van den Akker et al., 2025). An estimated ~ 8 mm increase in global mean sea level rise from WAIS mass loss between 1992 and 2017 was driven primarily by increased ice discharge in the Amundsen Sea drainage sector (Shepherd et al., 2018). To predict how Antarctica will respond to continued warming, it is vital to understand past ice sheet (in)stability during periods when the global climate was warmer than today.

One approach to understanding how ice sheets responded to past environmental change is to study the provenance of the detrital components in marine sediments. By determining where these sediments

* Corresponding author.

E-mail address: e.archibald22@imperial.ac.uk (E.J. Archibald).

<https://doi.org/10.1016/j.chemgeo.2026.123290>

Received 31 October 2025; Received in revised form 21 January 2026; Accepted 7 February 2026

Available online 8 February 2026

0009-2541/© 2026 The Authors. Published by Elsevier B.V. This is an open access article under the CC BY license (<http://creativecommons.org/licenses/by/4.0/>).

originated, past ice flow patterns and transport pathways of the detritus can be reconstructed. Provenance tools are most powerful when following a multi-proxy approach that integrates a range of complementary geochemical signatures (Licht and Hemming, 2017). For instance, geochronological techniques, such as zircon U-Pb dating and hornblende and biotite $^{40}\text{Ar}/^{39}\text{Ar}$ dating, determine individual ages of coarse-grained minerals (Roy et al., 2007; Pierce et al., 2011; Craddock et al., 2017a). Integrating such age data with isotope data analysed on the fine-grained detrital fraction creates an enhanced and often distinctive overall geochemical fingerprint, enabling more robust tracing of sediment sources (e.g., Simões Pereira et al., 2018) and transport histories of detritus which elucidates ice sheet dynamics through time (Marschalek et al., 2021).

An important prerequisite for unravelling past WAIS change using provenance data in marine sediments is detailed knowledge of West Antarctica's exposed and subglacial geology (e.g., Storey et al., 1994; Riley et al., 2020b). However, incomplete knowledge of isotopic source signatures across the continent is exactly where the effectiveness of the approach is hampered. The Ellsworth-Whitmore Mountains (EWM) crustal block is one example of such a poorly constrained source area. Located in a geologically sensitive position for recording WAIS retreat, it intersects the Amundsen, Ross, and Weddell Sea drainage sectors

(Fig. 1), making it a critical region of source rocks that are potentially identifiable in offshore sediment cores around West Antarctica.

The EWM crustal block is exposed primarily in the Ellsworth Mountains, which extend for 350 km in the Weddell Sea sector. The mountains comprise a 13 km thick succession of Pre-Cambrian to Permian conformable strata (Dalziel and Elliot, 1982; Webers et al., 1992; Curtis and Lomas, 1999; Castillo et al., 2024). The mountain range is bounded to the east and west by major topographic depressions and can be divided into the northern Sentinel Range and southern Heritage Range, separated by the eastward flowing Minnesota Glacier. The Ellsworth Subglacial Highlands extend for approximately 300 km to the South and West (Small et al., 2025). Previous studies of the Ellsworth Mountains have focussed on the tectonic evolution and history (Webers et al., 1992; Curtis, 2001; Flowerdew et al., 2007; Castillo et al., 2017; Craddock et al., 2017a; Castillo et al., 2024); the geochemical provenance signature of the modern mountain range and subglacial crustal block is yet to be characterised in detail, with a first attempt using Nd, Sr, and Pb isotope ratios recently reported by Horikawa et al. (2026). This block also includes the Mesozoic crystalline basement observed at Haag Nunataks (Fig. 1), which is distinct from the sedimentary succession of the Ellsworth Mountains. This displaced EWM crustal block has a complex tectonic history and has been rotated and translated to its current position (Jordan et al., 2020) and has a geological signature that is distinct from other sectors in West Antarctica and therefore provides a critical reference point for sediment provenance studies.

Modern ice flow trajectories inferred from satellite imagery indicate that, currently, detritus eroded from exposed and subglacial Ellsworth Mountains bedrock is primarily being transported out towards the Weddell Sea Embayment via the Rutford and Institute ice streams (Fig. 1). However, in previous warm periods such as the early to mid-Pliocene, ice sheet retreat could have radically altered transport pathways of glacially eroded detritus. In particular, the opening of seaways through West Antarctica (e.g. DeConto et al., 2021; Lau et al., 2023; Rahaman et al., 2025) would have provided new transport pathways for ice rafted debris. Understanding the past configurations of the WAIS in response to different climates is key to reducing uncertainties in ice-sheet model projections (DeConto et al., 2021; Golledge et al., 2021).

We here constrain the geochemical signature of samples from the EWM crustal bedrock. We determine the EWM provenance signature using strontium (Sr) and neodymium (Nd) isotope ratios (51 samples), magnetic mineral assemblages (45 samples), major element data (45 samples) and detrital zircon U-Pb ages (4 samples). Together these data help quantify the distinct provenance characteristics of each lithological group within the Ellsworth Mountains and permit identifying its provenance signature in studies of past WAIS configurations in marine sediment cores. Our new data also permit correlation of outlying nunataks, located further south and west, extending our provenance "fingerprint" to parts of the Ellsworth Subglacial Highlands. We present these results both in the context of the Ellsworth Mountains geological history and as an aid to understanding past WAIS dynamics.

2. Stratigraphy of the Ellsworth Mountains

2.1. Regional setting

West Antarctica consists of three main physiographic provinces: the Weddell Sea province, the West Antarctic Rift System & Marie Byrd Land, and the Antarctic Peninsula & Thurston Island (Jordan et al., 2020). The Weddell Sea province contains the oldest lithological units exposed in West Antarctica, including a Mesoproterozoic (c.1238 Ma) granodiorite gneiss complex at Haag Nunataks (Riley et al., 2020a) and Neoproterozoic (c. 682 Ma) diorite of the Ellsworth Whitmore Mountains (Castillo et al., 2024). This province is bound by the Antarctic Peninsula & Thurston Island to the north and East Antarctica to the south. The main ice sheet drainage basins in West Antarctica are the Weddell Sea, Ross Sea and Amundsen Sea sectors (Fig. 1), all of which

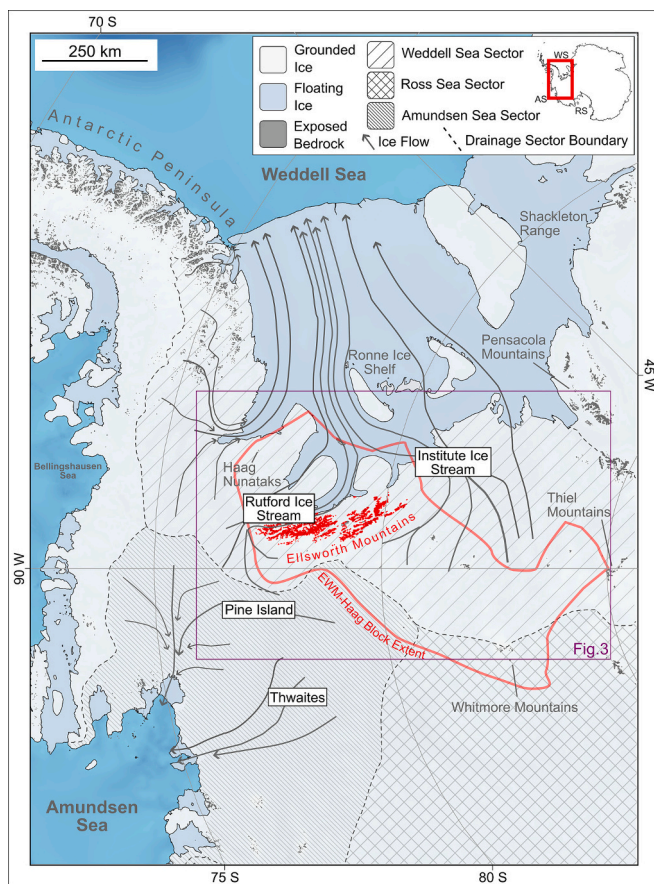


Fig. 1. Geological map of West Antarctica showing areas of grounded ice, floating ice shelves, exposed bedrock, major ice catchments and ice flowlines (Cox et al., 2023). Red bedrock shows the extent of exposed Ellsworth Mountains bedrock. Solid red line outlines the Ellsworth-Whitmore Mountains (EWM)-Haag block extent (Jordan et al., 2013). Basemap data from Quantarctica3 database (Matsuoka et al., 2018). WS = Weddell Sea, AS = Amundsen Sea, RS = Ross Sea. Transport of material from the Ellsworth Mountains to the Ross Sea is negligible under the modern ice configuration, and therefore the Ross Sea embayment is not included in the main map. (For interpretation of the references to colour in this figure legend, the reader is referred to the web version of this article.)

extend into the EWM-Haag region.

The Ellsworth Mountains present-day position lies approximately perpendicular to the neighbouring Transantarctic Mountains, which, together with palaeopole reconstructions, indicates post-depositional block rotation (Randall and Mac Niocaill, 2004; Watts and Bramall, 1981). Basement rocks are not exposed in the Ellsworth Mountains. Although a Precambrian basement is thought to underlie the EWM, aeromagnetic data suggests that it is distinct from the neighbouring Haag Nunataks (Garrett et al., 1987; Storey et al., 1988). The entire of the overlying Ellsworth Mountains sedimentary sequence is considered regionally conformable, despite local discontinuities.

2.2. Heritage group

The oldest sedimentary unit within the EWM block is the Heritage Group, (Figs. 2, 3) predominantly exposed within the Heritage Range (Webers et al., 1992). The sedimentary succession has long been considered to be Cambrian, but recent zircon U-Pb ages from a micro-diorite intrusion indicate that parts of the succession were deposited during the Cryogenian (ca. 682 Ma; Castillo et al. (2024)). Deposited in a continental rift basin, the Heritage Group marks a period of volcanic activity and crustal instability (Curtis, 2001). It is composed of a 7.5 km thick succession of tuff, lahar deposits, clastic and carbonate sediments (Craddock et al., 2017a; Webers et al., 1992; Jordan et al., 2020).

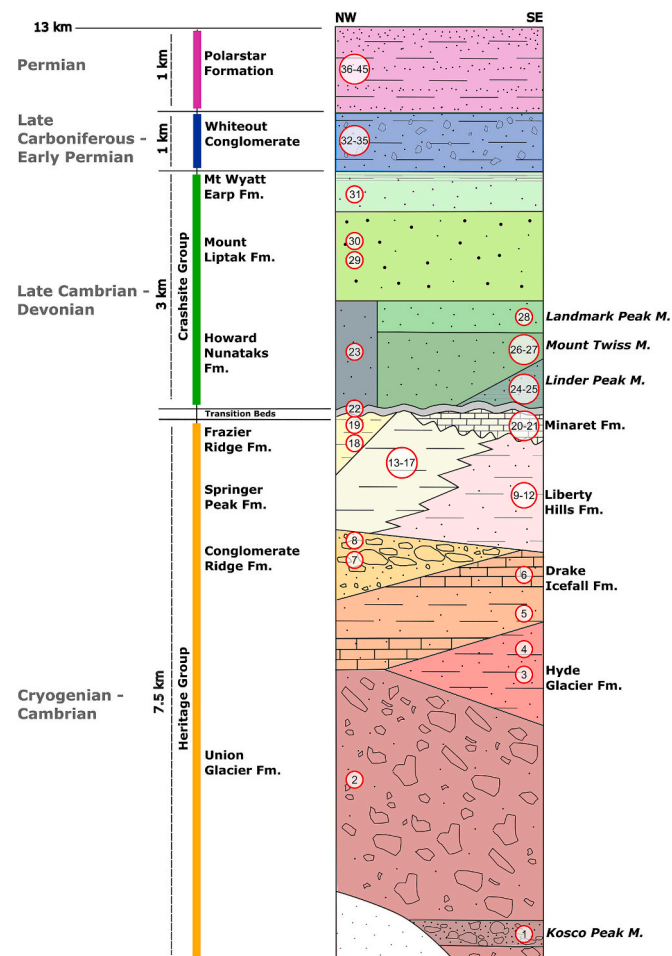


Fig. 2. Stratigraphic column of the Ellsworth-Whitmore mountains, edited from Webers et al. (1992). Sample numbers are in approximate stratigraphic position and correspond to those in Fig. 3 and Table S1, with details illustrated from the use of both hand specimen samples and sample collection field reports by Michael Curtis and Darren Randall (1993-1996).

2.3. Crashesite group

The conformable contact between the Heritage Group and the Crashesite Group can be seen in the Heritage Range (Webers et al., 1992). Continental rifting and alkaline magmatism ceased at the end of the Heritage Group deposition, with the remaining 5 km of the stratigraphy deposited under shallow marine environments (Webers et al., 1992).

The Crashesite Group is found extensively throughout the Ellsworth Mountains (Fig. 3), with thicknesses reaching up to 3 km in the Sentinel Range (Webers et al., 1992). The lithology is spatially and temporally less variable than that of the underlying Heritage Group. The Crashesite Group consists of Late Cambrian and Devonian strata predominantly comprised of quartzite, argillite, and conglomerate, with few limestones and igneous rocks, and was deposited during a period without major tectonic activity (Jordan et al., 2020).

2.4. Whiteout Conglomerate

The Crashesite Group gradually transitions into the overlying Whiteout Conglomerate, a 1 km thick diamictite succession deposited during the Late Carboniferous-Early Permian Gondwanan glaciation (Webers et al., 1992). Excluding the outcrops in the Meyer Hills, the Whiteout Conglomerate is restricted to the Sentinel Range of the Ellsworth Mountains, with its lithology varying significantly between outcrops (Webers et al., 1992). Diamictites of the Whiteout Conglomerate are separated by layers of shale, mudstone, and sandstone (Webers et al., 1992). Ice flow markers and distinct fossils (Jordan et al., 2020) allow correlation of these lithologies to units found in South Africa, the Falkland Islands, and the Pensacola Mountains located to the southeast of the Ronne Ice Shelf (Castillo et al., 2017; Craddock et al., 2017a).

2.5. Polarstar formation

Like the underlying units, the contact between the Polarstar Formation and the Whiteout Conglomerate appears transitional. Exposure of the youngest Polarstar Formation is confined to the NE Sentinel Range (Webers et al., 1992). The lowermost section of the Polarstar Formation contains mostly argillite that transitions into interbedded argillite and sandstone with coarsening upward sedimentary cycles, capped by coal measures at the top of the sequence (Castle and Craddock, 1975; Webers et al., 1992). Zircons from the Polarstar Formation show a close provenance relationship to late Permian units in the Falkland Islands, southern Africa and the southern Antarctic Peninsula (Riley et al., 2025).

2.6. Ellsworth Subglacial Highlands

Due to the dry and cold environment, the exposed Ellsworth Mountains are not being glacially eroded as rapidly as the subglacial bedrock beneath the fast-flowing ice streams. It is therefore important to also quantify the subglacial portion of the EWM block (Figs. 1 and 3), the only continuous topographic link between East and West Antarctica (Storey and Macdonald, 1987). Understanding its structure and composition provides a foundation for reconstructing past tectonic connections and transport pathways of detritus.

To do this we studied samples from isolated nunataks alongside published aerogeophysical data (airborne radar, aeromagnetic, aerogravity) to reveal the extent of the Ellsworth Mountains and distribution of their sedimentary strata (Jordan et al., 2013). Within the EWM block two main domains exist: 1) the Ellsworth domain, and 2) the Marginal domain, which are divided by the Pagano Shear Zone (Jordan et al. (2013), Fig. 3). In the Ellsworth domain, sedimentary rocks show NW-SE trending structures, whereas in the Marginal domain the sedimentary sequences are oriented NE-SW, suggesting they may contain elements of an older orogen (Storey and Macdonald, 1987).

Previous observations at these nunataks have found correlations

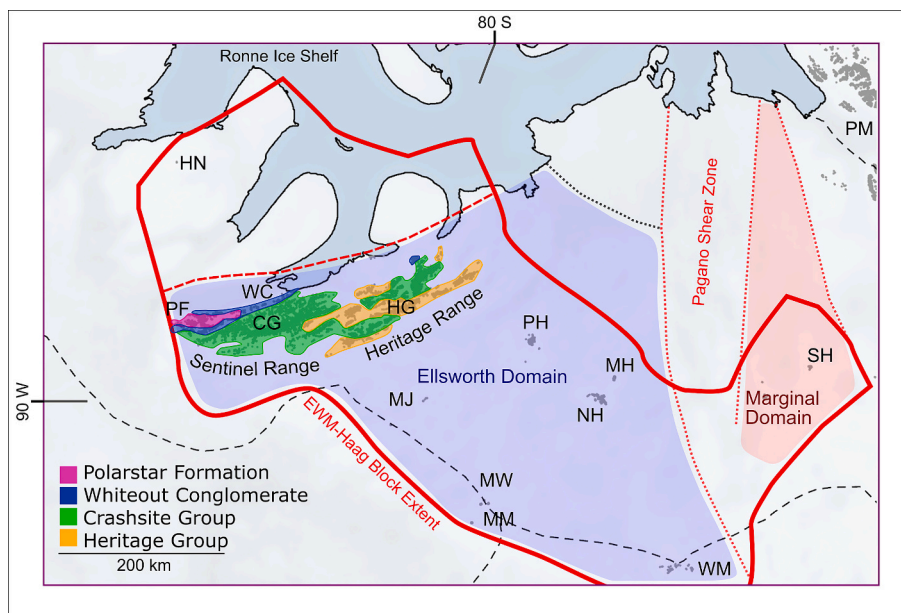


Fig. 3. Geological map and geophysically defined subglacial domains. *HG* = Heritage Group, *CG* = Crashesite Group, *WC* = Whiteout Conglomerate, *PF* = Polarstar Formation, *PH* = Pirrit Hills, *MH* = Martin Hills, *NH* = Nash Hills, *MJ* = Mount Johns, *MM* = Mount Moore (all this study), *MW* = Mount Woollard, *WM* = Whitmore Mountains, *SH* = Stewart Hills, *HN* = Haag Nunataks, *PM* = Pensacola Mountains, *EWM* = Ellsworth-Whitmore Mountains. *EWM-Haag* block extent and Ellsworth and Marginal domain from (Jordan et al., 2013), dashed line divides *EWM* and Haag extent.

with neighbouring tectonic units (Storey and Macdonald, 1987). Primarily, two main units have been identified in the nunataks of the Ellsworth domain, both of which have been correlated to the Heritage and/or Crashesite groups of the Ellsworth Mountains. This agrees with published correlations, based on U-Pb geochronology and Hf isotope analysis, which have linked outcrops from the Whitmore Mountains and Mt. Woollard to the Frazier Ridge Formation of the Heritage Group (Flowerdew et al., 2007).

A mixed clastic/carbonate unit has been reported at Nash Hills and Martin Hills containing limestone, calcareous sandstone and argillite (Fig. 3; Storey and Macdonald (1987)). Possible associated clastic/carbonate units in the Ellsworth Mountains include the Union Glacier Formation, the Drake Icefall Formation, and the Minaret Limestone. Contact metamorphism has been identified throughout the Nash Hills and Martin Hills area and is attributed to the emplacement of large Middle Jurassic granite plutons (Storey and Macdonald, 1987). Although intrusive rocks are present in the *EWM*, they are not discussed further due to their limited surface exposure. Additionally, Jurassic granites, which yield zircon U-Pb ages between 170 Ma and 200 Ma, are observed in various locations around West Antarctica (Pankhurst et al., 1993; Craddock et al., 2017b; Jordan et al., 2025). They are therefore not unique to the Ellsworth Mountains, and so they cannot be used to build a distinct provenance fingerprint.

The Mt. Johns Formation, a red sandstone unit, is found at several nunataks to the SSW of the Ellsworth Mountains, including Mt. Johns, Pirrit Hills and Mt. Moore (Fig. 3), with each outcrop thought to represent a separate exposure of this sedimentary unit. The facies types in the Mt. Johns Formation include sand, mud and silt, suggesting fluvial deposition on a low-relief surface, typical of ephemeral braid plains (Storey and Macdonald, 1987). Based on sedimentary facies, correlative units exposed in the Ellsworth Mountains may include the Hyde Glacier Formation, the Springer Peak Formation, and the Crashesite Group quartzites.

3. Samples and methods

For this study, a series of geochemical analyses was conducted on 45 bedrock samples from the Ellsworth Mountains and six samples from

isolated nunataks to the SSW of the Ellsworth Mountains (Table S1; Figs. 3, 4). Most samples originated from sedimentary or low-grade metamorphic rocks; however, eight were from igneous or higher-grade metamorphic rocks of the Heritage Group. Samples were sourced from the rock repository of the British Antarctic Survey (BAS) in Cambridge (UK) and were originally collected during field expeditions between 1983 and 1996. Samples were chosen based on their geographic and stratigraphic position. Where possible, all major facies within each lithological group were sampled. Nunatak rock units were chosen based on field observations (Storey and Macdonald, 1987), and their rock unit and regional correlations were assessed.

Initial separation and crushing of the bulk rock samples took place at the BAS. Samples were sieved and powdered in preparation for a range of different analyses. Methods and results of the magnetic mineralogical analyses are provided in the Supplementary Information. Previously cored sections of the Whiteout Conglomerate used for palaeomagnetic investigations were analysed in this study. These diamictites are composed of predominantly quartz clasts (< 10 mm) within a grey-black silt-clay matrix. In all cases, the entire core section was crushed and powdered to produce a homogeneous sample. This approach ensured the sample material was representative of the unit, rather than biasing towards larger clasts (> 10 mm), which form <5% of the Whiteout Conglomerate.

3.1. Neodymium and strontium radiogenic isotope analysis

All Ellsworth Mountains and nunatak (Mt. Johns, Mt. Moore, Pirrit Hills, Nash Hills, Martin Hills; Fig. 3) samples were measured for their radiogenic Nd and Sr isotope signatures. Analyses were carried out on 50 mg aliquots of the fine-grained bulk rock powder. A mixture of concentrated HNO₃ (1 ml), HClO₄ (0.8 ml), and HF (2 ml) was used to digest the samples in Savillex vials on a hotplate (120 °C) for 3 to 5 days. Samples were converted into chloride-form following complete dissolution, and Nd and Sr were isolated from the rock matrix using a three-stage ion exchange chromatography. In a first stage, rare earth elements (REE) and Sr were separated from the sample matrix using cation exchange resin (AG50W X-8, 200–400 μm mesh) and HCl in increasing molarity. Neodymium was then separated from the other REEs using Ln-

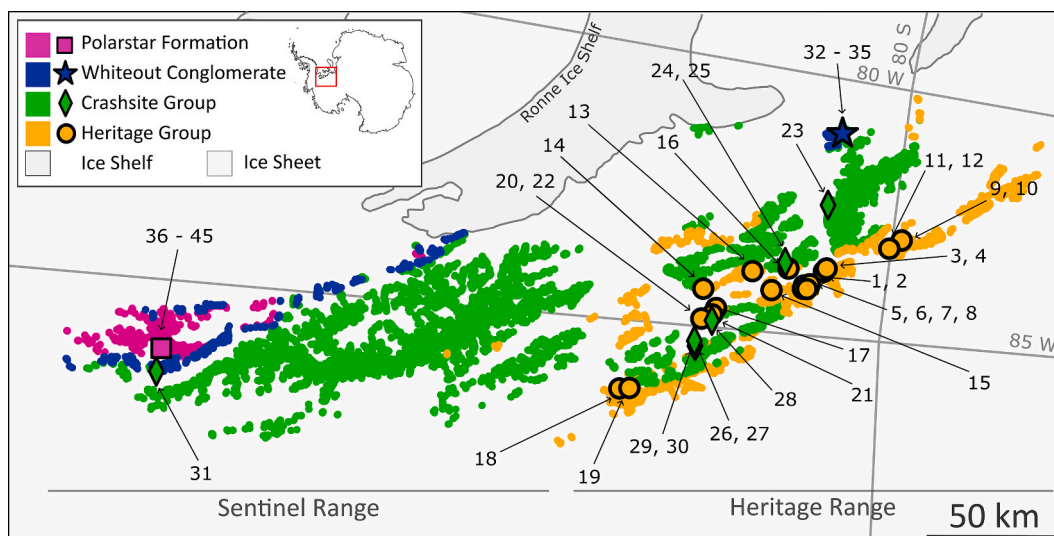


Fig. 4. Sample location map of sedimentary units and sample sites within the Ellsworth-Whitmore Mountains. Numbered sites correspond to those in Table S1.

spec resin (50–100 μm) and low molarity HCl. The sample matrix from the cation exchange step was dried and taken up in HNO_3 and loaded onto Eichrom Sr-spec resin to isolate Sr by elution with water.

Neodymium isotopes were measured on a Nu Plasma HR MC-ICP-MS in the MAGIC laboratories at Imperial College London (UK). Instrumental mass bias was corrected for using a known $^{146}\text{Nd}/^{144}\text{Nd}$ ratio of 0.7219 and an exponential law. Although negligible, interferences of ^{144}Sm on ^{144}Nd were corrected for. Measured $^{143}\text{Nd}/^{144}\text{Nd}$ ratios were corrected using bracketed JNdi $^{143}\text{Nd}/^{144}\text{Nd}$ ratios and the accepted ratio of 0.512115 (Tanaka et al., 2000). Six procedural Nd blanks were below 61 pg, with five showing Nd concentrations of <20 pg, corresponding to a maximum blank contribution of 0.04% of the sample signal, which is negligible. Repeat measurements of the USGS BCR-2 standard yielded results within error of the published $^{143}\text{Nd}/^{144}\text{Nd}$ ratio of 0.512638 ± 0.000015 (Weis et al., 2006), with an average $^{143}\text{Nd}/^{144}\text{Nd}$ ratio of 0.512640 ± 0.000016 (2SD, $n = 36$). Neodymium isotope ratios are expressed as epsilon values (ϵ_{Nd}), which denotes the deviation of a measured $^{143}\text{Nd}/^{144}\text{Nd}$ ratio from the Chondritic Uniform Reservoir (CHUR) ratio of 0.512638 in parts per 10^4 (Jacobsen and Wasserburg, 1980).

Dried Sr fractions were redissolved in 10 μl 6 M HCl of which 1 μl was loaded onto degassed tungsten filaments, coated with 1 μl of TaCl_5 activator. Carbonate samples were redissolved in 30 μl to account for higher Sr concentrations. Strontium isotope ratios were measured using a Triton Thermal Ionisation Mass Spectrometer (TIMS) in the MAGIC laboratories. Measured $^{87}\text{Sr}/^{86}\text{Sr}$ ratios were corrected for mass bias using an exponential law and an $^{88}\text{Sr}/^{86}\text{Sr}$ ratio of 8.375. Interferences of ^{87}Rb were corrected using an $^{87}\text{Rb}/^{85}\text{Rb}$ ratio of 0.386. Analyses of the NIST 987 standard, yielded a mean $^{87}\text{Sr}/^{86}\text{Sr}$ ratio of 0.710245 ± 0.000012 (2SD, $n = 61$), and samples were corrected to a ratio of 0.710252 ± 0.000013 (Weis et al., 2006). Accuracy of results was confirmed by repeat analysis of USGS BCR-2 standard, yielding $^{87}\text{Sr}/^{86}\text{Sr}$ ratios of 0.705006 ± 0.000013 (2SD, $n = 21$), which is within error of the published ratio of 0.705013 ± 0.000010 (Weis et al., 2006). Procedural blanks ranged between ~ 100 pg and ~ 900 pg, which is negligible ($< 0.05\%$ assuming upper continental crust Sr concentrations).

3.2. Zircon U-Pb ages

Zircon U-Pb ages were determined on four of the nunatak samples (Mt. Johns, Mt. Moore, Pirrit Hills, Martin Hills; Fig. 3). We did not collect any additional U-Pb data from the main Ellsworth Mountains

region as the bedrock zircon geochronology is well characterised (Flowerdew et al., 2007; Elliot et al., 2015; Castillo et al., 2017; Craddock et al., 2017a; Castillo et al., 2024).

Nunatak samples were crushed and sieved to $< 500 \mu\text{m}$. Zircons were isolated from this fraction using standard heavy liquid and magnetic separation techniques, then mounted on glass slides, set in resin, and polished until zircon surfaces were exposed. Apatite U-Pb dating at University College London was performed using an Agilent 7900 ICP-MS coupled to an ESI/New Wave Research NWR193 laser system equipped with an ATLEX I LR laser source (~ 5 ns pulse width) and a TV2 ablation cell. The laser was operated at 10 Hz for 30 s per spot, including 5 s of background measurement, with a 25 μm spot diameter and an energy density of 2.2 J/cm^2 at the sample surface. Ablation occurred in a 100% helium atmosphere flowing at 1.05 L/min through the ablation cell. Helium was mixed with argon halfway along the sample transport line to the torch via a Y-piece. The plasma was sustained at 1400 W RF power. Ions were analysed on a single-collector SEM operating in pulse or analog mode, scanning masses 29 (12 ms), 91 (2 ms), 139 (5 ms), 206 (50 ms), 207 (60 ms), 208 (40 ms), 232 (20 ms), 235 (20 ms) and 238 (20 ms).

The mass spectrometer was tuned by drawing a 50 μm line on NIST 612 glass, using a fluence of 3.5 J/cm^2 . This gave $^{248}\text{ThO}/^{232}\text{Th}$ values of $< 0.2\%$ (oxide production), $^{232}\text{Th}/^{238}\text{U}$ values of $> 90\%$ (fractionation), and 20,000 counts per second of ^{238}U .

Plesovice zircon (Sláma et al., 2008) served as the primary reference material, and GJ-1 (Jackson et al., 2004) and 91500 zircon (Wiedenbeck et al., 2004) as the secondary (validation) standards. Data acquisition was carried out using Agilent MassHunter software, isotopic ratios were calculated with GLITTER 4.5 (Griffin et al., 2008), and post-processing was performed in IsoplotR 6.6 (Vermeesch, 2018). GJ-1 apatite analyses yielded a weighted mean age of 599 ± 2 Ma (MSWD = 1.3, $n = 44$), and 91500 zircon a weighted mean age of 1051.6 ± 3.9 Ma (MSWD = 0.82, $n = 42$). All zircon U-Pb ages used in this study, including those from the literature, have been corrected for common lead and further filtered to remove discordant results using a concordia distance threshold (Vermeesch, 2021b).

3.3. Scanning electron microscopy

Major oxide compositions were determined for all 45 EWM bedrock samples. 1–2 cm^3 sample chips were mounted in epoxy set into circular moulds and cut into 1 cm thick pucks using a precision saw. Cut surfaces were polished and carbon coated before introduction into the Zeiss Evo

MA 15 scanning electron microscope housed at CASP (Cambridge, UK). Back scattered electron (BSE) images and elemental maps were collected using a Zeiss BSE detector and an Oxford Instruments Ultim Max 100 Energy dispersive x-ray spectrometer (EDS) detector. The instrument was set up at 20 kV and 2000 pA i-probe, with an BSE and EDS resolution of 1 μm and 2 μm , respectively. Montages of BSE and EDS images cover 5 mm^2 representative areas for each sample, from which proxy whole rock major elemental compositions and mineralogy were determined. The elemental data were collected using the “standardless” approach developed by Oxford Instruments and detailed by (Pinard et al., 2020). To check the detector- and instrument-specific calibration is appropriate, beam measurements on pure copper were carried out before each analytical session to ensure that the beam was stable and as sensitive as previous sessions under identical conditions. In addition, accuracy was monitored against an internal sample where XRF major-element geochemistry exists. Images and data were collected, manipulated and exported using Oxford Instruments AZtec software version 6.1.

4. Results

Below we present lithology, bulk rock radiogenic isotope data, and U-Pb zircon ages to characterise the EWM block. Data on magnetic measurements (methods and results) conducted on all 45 EWM bedrock samples are provided in the Supplementary Information. Magnetic mineralogical analyses did not contribute additional constraints on the sediment provenance fingerprint due to variability being confined to the Heritage Group and the weakly magnetic nature of the samples.

4.1. Major element geochemistry

Elemental compositions vary up-stratigraphy, consistent with the geological development of the basin. These variations are illustrated using the analysis of Lipp et al. (2020), (Fig. 5, Table S2). The Heritage Group displays highly variable compositions, derived from a mixture of felsic and mafic sources, and records a range of chemical weathering intensity experienced. In contrast, the younger strata show a systematic reduction in the intensity of chemical weathering, coupled with changes in the composition of the crystalline source rocks from which they were derived. Sediments of the Crashsite Group were derived from moderately felsic sources and experienced high degrees of chemical weathering and are compositionally mature with high detrital quartz contents (Table S2). The Whiteout Conglomerate diamictites originate from more mafic sources and record a reduction in chemical weathering intensity,

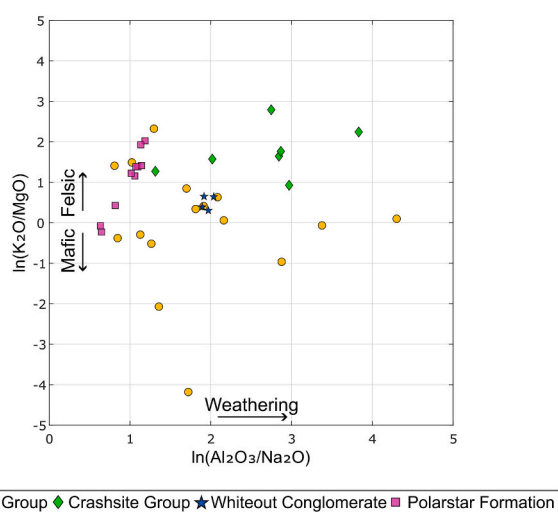


Fig. 5. Illustration of rock composition and degree of weathering for the Ellsworth Mountains samples. $\ln(\text{K}/\text{Mg})$: proxy for felsic (>0) and mafic (<0) sources; $\ln(\text{Al}/\text{Na})$: proxy for weathering (Lipp et al., 2020).

consistent with their deposition in a glacial setting with dominance of physical weathering. This trend continues into the Polarstar Formation, which experienced the least chemical weathering and has the strongest felsic source signal. Both the Whiteout Conglomerate and Polarstar Formation are characterised by little variability in their Al/Na ratios.

4.2. Neodymium and strontium isotope composition

The Nd isotope compositions of Ellsworth Mountains bedrock samples vary between ϵ_{Nd} values of +2.5 and -18.5 , with corresponding $^{87}\text{Sr}/^{86}\text{Sr}$ ratios from 0.705 to 0.762 (Fig. 6, Table S2). When considering both radiogenic isotope systems, each lithological group shows a distinct fingerprint (Fig. 6). The clear outlier in the data set in terms of its Nd isotope composition is a sill sample from the Heritage Group, which matches the range observed in previously analysed sill samples and is thought to result from the later intrusion of these sills from a different magma source (Curtis et al., 1999). This sample is the only one measured in this study with a positive ϵ_{Nd} value (Fig. 6). As the lithology of the sill sample only represents a very minor fraction of the exposed geology, the result is omitted from further characterisation of the Heritage Group.

The next highest ϵ_{Nd} values were observed in the youngest group, the Polarstar Formation, which yielded a well-defined data cluster around $\epsilon_{\text{Nd}} = -3.8$ to -4.9 and $^{87}\text{Sr}/^{86}\text{Sr} = 0.709$ to 0.715. At the other end of the Nd isotope spectrum, the lowest ϵ_{Nd} values are recorded in the underlying Whiteout Conglomerate ($\epsilon_{\text{Nd}} = -17.5$ to -18.5 ; $^{87}\text{Sr}/^{86}\text{Sr} = 0.723$ to 0.729). The older Heritage and Crashsite groups show more internal heterogeneity, particularly in Sr isotope composition, with ϵ_{Nd} values ranging from -5.2 to -11.9 and -9.6 to -13.1 and $^{87}\text{Sr}/^{86}\text{Sr}$ isotope ratios ranging from 0.705 to 0.753 and 0.723 to 0.762, respectively (Fig. 6).

The samples from the nunataks either fall within the field of the Heritage Group samples (clastic/carbonate samples from the Nash Hills and the Martin Hills; $\epsilon_{\text{Nd}} = -7.2$; $^{87}\text{Sr}/^{86}\text{Sr} = 0.716$ to 0.717) or at the transition of the Heritage and Crashsite groups (sandstone samples from the Pirrit Hills, Mt. Moor and Mt. Johns; $\epsilon_{\text{Nd}} = -9.3$ to -10.6 ; $^{87}\text{Sr}/^{86}\text{Sr} = 0.727$ to 0.745) (Fig. 6).

4.3. Nunatak zircon U-Pb age signature

Our new detrital zircon U-Pb dates of the samples from Martin Hills ($n = 83$) and Pirrit Hills ($n = 115$) are characterised by two approximately equal age peaks, centred around 1100 Ma and 520 Ma. Samples from Mt. Johns ($n = 83$) have a dominant age peak at c. 530 Ma, but with a minor age peak at c. 1000 Ma, whereas the Mt. Moore sample ($n = 136$) has a dominant age peak at c. 1000 Ma (Fig. 7a). In contrast, zircon U-Pb ages previously reported for granitic rocks from the nunataks of the EWM block are centred at c. 170 Ma and 200 Ma (Craddock et al., 2017b).

5. Discussion

5.1. Sediment provenance characteristics of the exposed Ellsworth Mountains

Previous studies have shown that different lithologies within the Heritage Group exhibit different zircon U-Pb age spectra (Fig. 7). In most cases, the older Heritage Group samples (e.g. Kosco Peak) are dominated by Grenville Orogeny ages (1000–1250 Ma), whereas the younger Heritage Group samples (e.g. Springer Peak and Frazier Ridge) tend to show a bimodal distribution of Grenville Orogeny ages and Ross Orogeny (480–590 Ma) and/or Pan-African Orogeny ages (500–650 Ma) (Flowerdew et al., 2007; Castillo et al., 2017). Combined, the Heritage Group contains Grenville Orogeny zircon U-Pb ages approximately five times more abundant than Ross Orogeny ages (Flowerdew et al., 2007; Castillo et al., 2017; Castillo et al., 2024; Figs. 7, 8). We estimate the

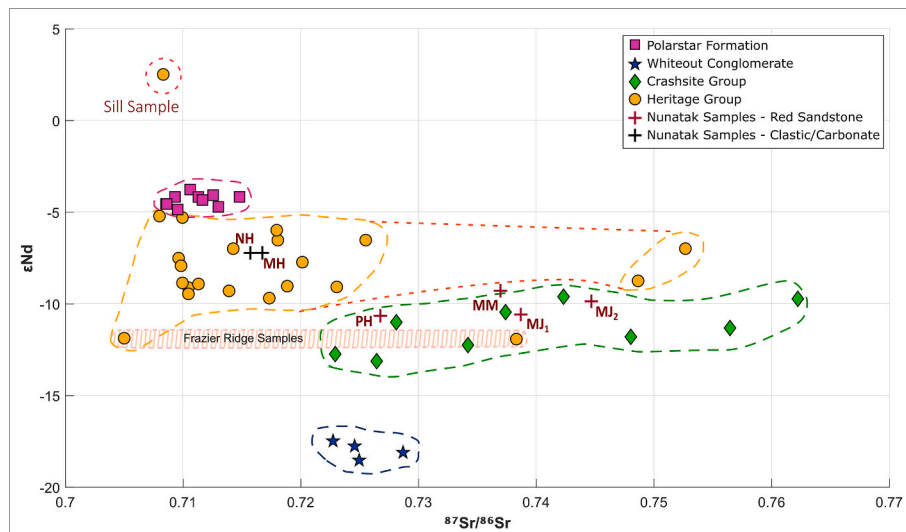


Fig. 6. Neodymium and strontium isotope compositions of all Ellsworth-Whitmore Mountain samples from this study. Nunatak locations are abbreviated as follows: NH = Nash Hills, MH = Martin Hills, PH = Pirrit Hills, MM = Mt. Moore, MJ_{1,2} = two samples from Mt. Johns.

maximum depositional age (MDA) of the youngest Heritage Group strata using the maximum likelihood age (MLA) algorithm of Vermeesch (2021a). The MLA approach models the detrital zircon U-Pb age spectrum as a two-component mixture comprising (i) a discrete peak representing the depositional age and (ii) a continuous population of older ages described by a truncated normal distribution. Although this parametric formulation is necessarily simplified, the MLA algorithm has been shown to yield more accurate depositional age estimates than commonly used heuristic MDA methods (Vermeesch, 2021a). Applying the MLA method as implemented in IsoplotR v6.6 (Vermeesch, 2018), we obtain an MDA for the Heritage Group of 518 ± 7 Ma. The Heritage Group samples show the largest range in both isotope compositions and major element geochemistry, with ϵ_{Nd} values between -5.2 and -11.9 , and $^{87}Sr/^{86}Sr$ ratios from 0.705 to 0.753 (Figs. 6, 8). The data have given rise to suggestions of multiple original geological sources for these sediments, with agreement that the mountain region was located to the north of its current position during the Cambrian Period, likely receiving material from Gondwana (Flowerdew et al., 2007; Castillo et al., 2017; Randall et al., 2000; Randall and Mac Niocaill, 2004).

The overlying Crashsite Group can be distinguished by its detrital zircon U-Pb ages, with Ross Orogeny ages being twice as abundant as Grenville Orogeny ages, and an MLA of 422 ± 10 Ma (Figs. 7, 8). $^{87}Sr/^{86}Sr$ ratios range between 0.723 and 0.762, and ϵ_{Nd} values span -9.6 to -13.1 (Figs. 6, 8). The Crashsite Group is characterised by elevated Al/Na ratios in comparison to the younger overlying units, consistent with significant chemical weathering, sediment recycling and compositional maturity (Fig. 5).

The Whiteout Conglomerate zircon U-Pb age profiles do not differ notably from those of the underlying Crashsite Group (Fig. 7). However, they have distinct Nd and Sr isotope compositions, with highly unradiogenic ϵ_{Nd} values of -17.5 to -18.5 and $^{87}Sr/^{86}Sr$ values between 0.723 and 0.729 (Figs. 6, 8), suggesting that while the sediments were derived from a source of similar crustal age, they originated from distinct bedrock units within that source region, reflecting spatial and lithological variability. The Whiteout Conglomerate samples show an increase in mafic compositions and a drop in chemical weathering intensity in comparison to the underlying Crashsite Group (Fig. 5).

This contrasts with samples from the youngest (late Permian) Polarstar Formation, which have the highest ϵ_{Nd} values, ranging from -3.8 to -4.9 , and $^{87}Sr/^{86}Sr$ values from 0.709 to 0.715 (Figs. 6, 8). Zircon U-Pb ages are distinct for this formation because they predominantly show a strongly unimodal age distribution, with a peak at c. 270 Ma (Figs. 7, 8), and an MLA of 264 ± 1 Ma. Major element geochemistry

illustrates that this is the least chemically weathered unit and has the highest proportion of felsic sources in the EWM stratigraphy (Fig. 5).

5.2. Nunatak sedimentary unit correlations and implications for subglacial geology

Our new characterisation of the exposed geology of the Ellsworth Mountains combined with previously published zircon U-Pb data permits improved correlation of our sedimentary nunatak rock samples (to the SSW of the Ellsworth Mountains) to the main stratigraphy. This helps constrain the subglacial extent of the different rock groups. All nunataks investigated in this study are located within the Ellsworth domain (Fig. 3), which also includes the more distal Whitmore Mountains (Fig. 9).

In contrast to their similar lithology, all three red sandstone samples from the nunataks (Mt. Johns, Mt. Moore, Pirrit Hills) have distinct characteristics, indicating their different positions in the EWM stratigraphy (Figs. 6 and 7). The dominant Ross Orogeny age peak in the Mt. Johns sample resembles that of rocks from either the Crashsite Group or Whiteout Conglomerate (Fig. 7). However, the radiogenic isotope compositions of both samples from the Mt. Johns nunatak fall within the range of the Crashsite Group (Figs. 6 and 9), making it our preferred regional correlative.

The outlying nunatak located at Mt. Moore yields a zircon age distribution dominated by Grenville-aged zircons, indicating a likely correlation with the Heritage Group (Fig. 7). This is supported by the radiogenic isotope compositions, which fall within the values observed in the Heritage Group (Fig. 6). In contrast, the adjacent Mt. Woollard sample displays a distinct zircon age signature characteristic of the Crashsite Group (Flowerdew et al., 2007, Fig. 8).

The red sandstone sample from the Pirrit Hills exhibits approximately equal contributions from the Ross- and Grenville-aged zircon populations. This is a pattern also observed in the upper Heritage Group (Fig. 7). The radiogenic isotope composition of the Pirrit Hills sample falls between those of the Heritage and Crashsite groups, but more significantly, between those of the two Frazier Ridge samples (Fig. 6). The Pirrit Hills nunatak is therefore tentatively correlated to the Frazier Ridge Formation of the upper Heritage Group.

Similar to the Pirrit Hills sample, the bimodal distribution of zircon ages in the mixed clastic/carbonate sample at Martin Hills is indicative of the upper Heritage Group, which is consistent with the Frazier Ridge Formation or laterally equivalent Springer Peak Formation (Fig. 7). Whilst the zircon U-Pb age profile of the Martin Hills unit also resembles

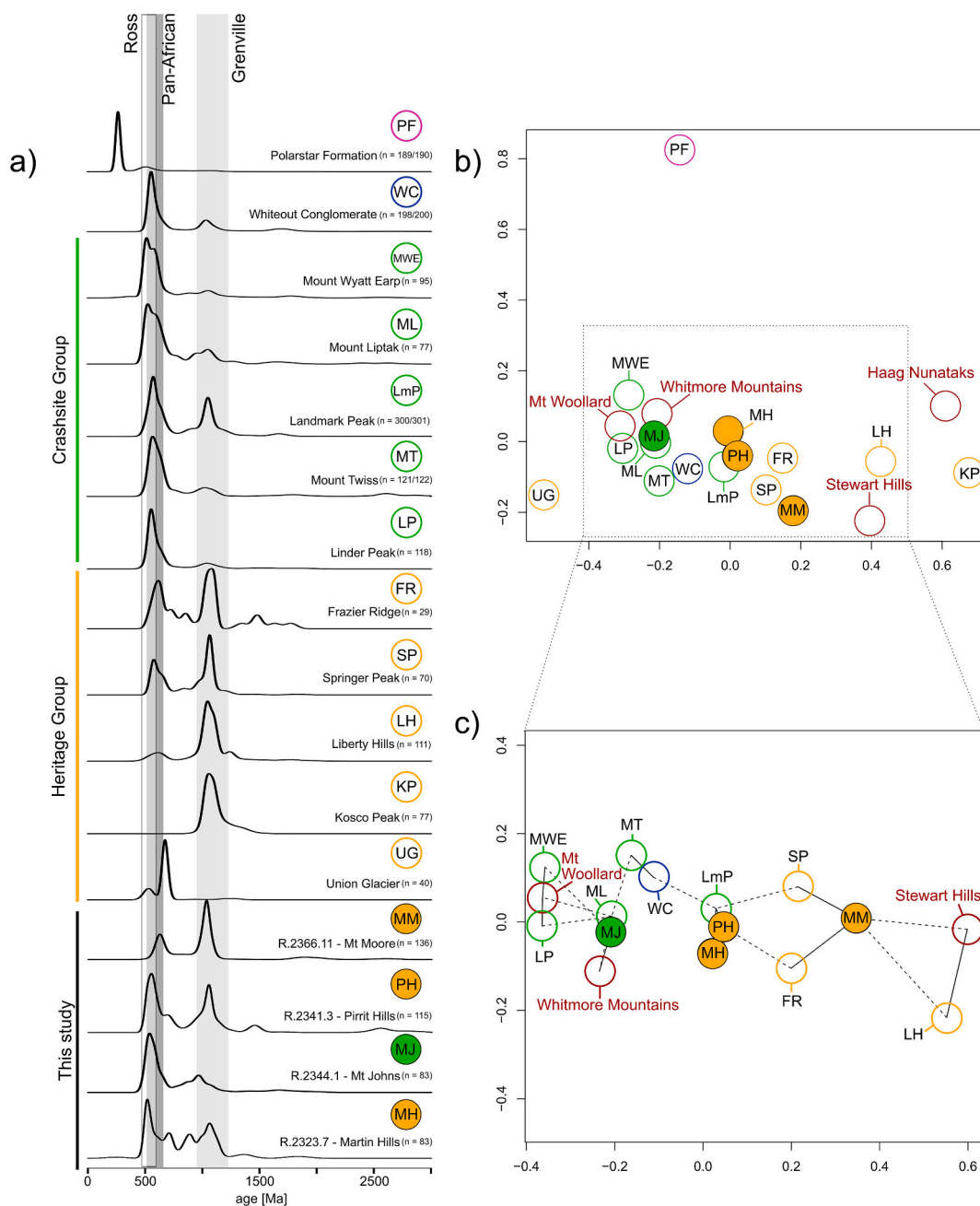


Fig. 7. Age and isotopic clustering across the Ellsworth-Whitmore Mountains. a) Literature zircon U-Pb data displayed as kernel density estimates (KDEs), calculated using a bandwidth of 30 Ma and bin width of 25 Ma, following Castillo et al. (2017). Grenville (1000–1250 Ma), Pan-African (500–650 Ma), and Ross Orogeny (480–590 Ma) illustrated in grey bars. Samples from this study highlighted by solid icons. b) Study sites and published zircon U-Pb ages displayed as a multidimensional scaling map (MDS). Proximity of data to each other reflects their similarities. Colours of sample sites according to lithological group, consistent with previous figures. Literature data are indicated by symbols with coloured outline, data from samples analysed in this study are indicated by filled symbols. c) MDS analysis using subset of data displayed in b), both from Vermeesch (2018), using the Kolmogorov-Smirnov dissimilarity measure. Solid and dashed lines in c) represent the nearest and second nearest neighbours in Kolmogorov-Smirnov space, as explained by (Vermeesch, 2013).

the Landmark Peak sample from the Crashesite Group (Fig. 7), this correlation is discounted because the Nd and Sr isotope signatures of the Martin Hills sample fall within the range of the Heritage Group (Figs. 6 and 7). Instead, we consider the Springer Peak Formation to be the most likely regional correlative for the samples from the Martin Hills.

The Nash Hills nunatak was not selected for zircon U-Pb analysis. However, as it is thought to belong to the same clastic/carbonate unit as the Martin Hills sample, and both display similar Nd and Sr signatures, the Nash Hills nunatak has also been correlated with the Heritage Group.

By comparing the new geochemical and geochronological data from the nunataks in the EWM crustal block with the main exposed mountain

range, we identify likely correlations with established geological units. While representing different positions within the stratigraphy, samples from Martin Hills, Nash Hills, Pirrit Hills and Mt. Moore display signatures consistent with the Heritage Group, whereas samples from the Mt. Johns nunatak predominantly indicate a correlation with the Crashesite Group (Fig. 8). These findings improve our understanding of the sub-glacial geology and provide a foundation for future sediment provenance studies.

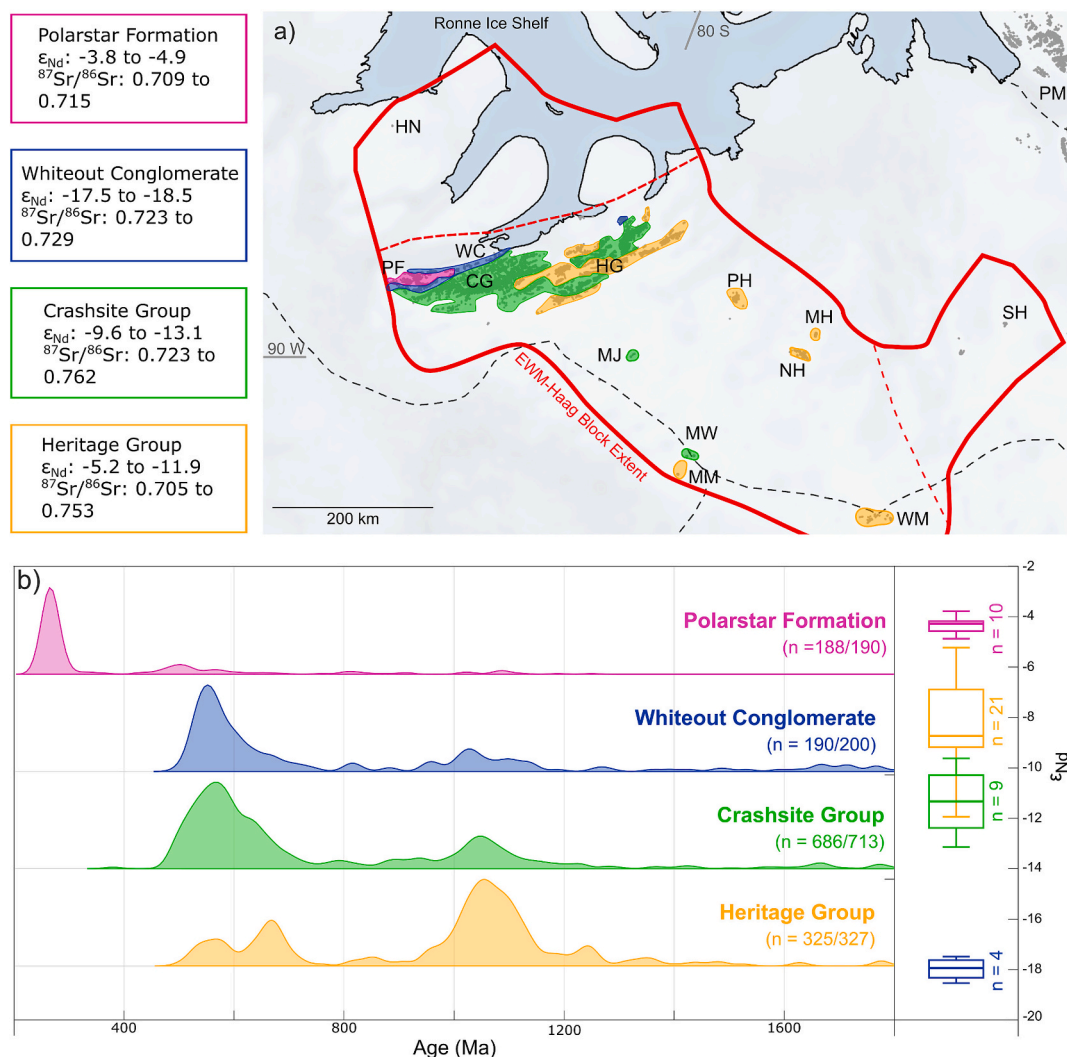


Fig. 8. Summary figure of the main provenance characteristics of the Ellsworth Mountains stratigraphic units. a) Geological map with interpreted nunatak geology. Colours represent lithological group, as displayed in previous figures. b) KDE plot of zircon U-Pb compilation of exposed Ellsworth Mountain bedrock from literature data (Fig. 7), using a bandwidth of 15 Ma, and box plots of measured ϵ_{Nd} from the exposed Ellsworth Mountain bedrock (this study).

5.3. Modern provenance signature of the Ellsworth-Whitmore Mountains crustal block

The EWM crustal block is located in a region that may have been the source for detritus discharged into the Weddell, Amundsen, Bellingshausen, and even Ross seas at times when the WAIS was less extensive than at present. Using our new bedrock data, we first establish whether the EWM signature is eroded and transported to the ocean in a modern ice sheet configuration.

By assigning the geological composition of the nunataks to either the Crashsite or upper Heritage groups, we infer that much of the Ellsworth Subglacial Highlands comprises of rocks from these groups. Based on aerial extent, we expect the Whiteout Conglomerate and Polarstar Formation to make up <10% of the Ellsworth domain provenance signature. Therefore, detritus eroded from the Ellsworth domain would, if mixed, likely be characterised by bimodal zircon U-Pb age profiles with both Grenville and Ross orogeny populations, as well as mean ϵ_{Nd} values of ~ -10 and $^{87}Sr/^{86}Sr$ ratios of ~ 0.728 . This calculation assumes equal Nd and Sr concentrations and a 10% weighted mean of Lower Heritage Group, Whiteout Conglomerate and Polarstar Formation, with 90% weighted average from 50% Crashsite and 50% Upper Heritage Group (Fig. 10, Table S3).

Ice flow velocities derived from satellite imagery suggest the two

main transport routes from the EWM towards the Weddell Sea at present are the Rutford Ice Stream and the Institute Ice Stream (Fig. 1). There are no data to directly constrain the isotopic provenance signature of Institute Ice Stream. However, the modal zircon U-Pb age peaks of 560 Ma and 1100 Ma recorded in moraines adjacent to the ice stream (Agrios et al., 2021) suggest that the eroded material likely originates from the Ellsworth Subglacial Highlands, particularly from the proximal nunataks at Pirrit Hills, Nash Hills and Martin Hills. Our new characterisation of these nunataks suggests that their provenance signature is consistent with that of the upper part of the Heritage Group; i.e. a mean ϵ_{Nd} value of approximately -9 (full ϵ_{Nd} range: -5 to -12) and mean $^{87}Sr/^{86}Sr$ ratio of ~ 0.717 (full $^{87}Sr/^{86}Sr$ range: 0.705 to 0.753). This signature represents an equal contribution of detritus from Liberty Hills, Springer Peak, Frazier Ridge, and Minaret formations (Figs. 8 and 10). The catchment of the Rutford Ice Stream includes the Sentinel Range of the Ellsworth Mountains (King, 2009, Fig. 1). The provenance signature of detritus eroded by the Rutford Ice Stream would, based on our new characterisation, be dominated by a Crashsite Group signature, with average ϵ_{Nd} values of approximately -12 (ϵ_{Nd} range of -10 to -13) and mean $^{87}Sr/^{86}Sr$ ratios of ~ 0.740 ($^{87}Sr/^{86}Sr$ range of 0.723 to 0.762) (Table S3).

The catchment of Pine Island Glacier, which drains into the Amundsen Sea, currently extends into the EWM block region (Figs. 1, 2).

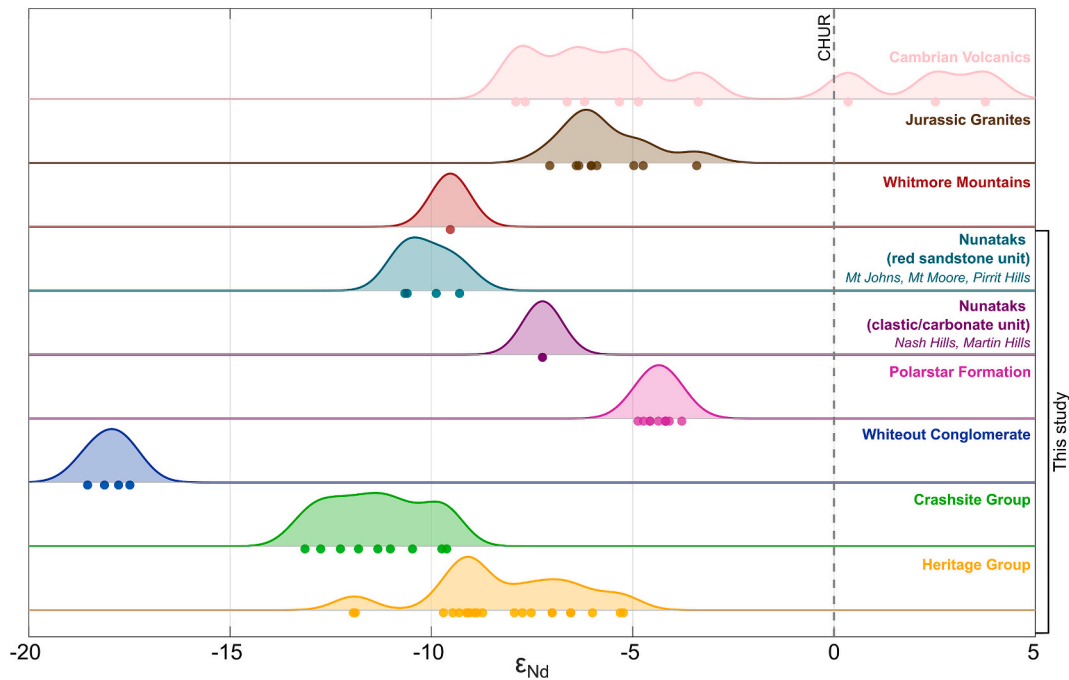


Fig. 9. KDE plots for published whole-rock ϵ_{Nd} values from West Antarctica (Curtis and Lomas, 1999; Craddock et al., 2017b; Marschalek et al., 2021; Horikawa et al., 2026) compared to new results from this study. CHUR = chondritic uniform reservoir.

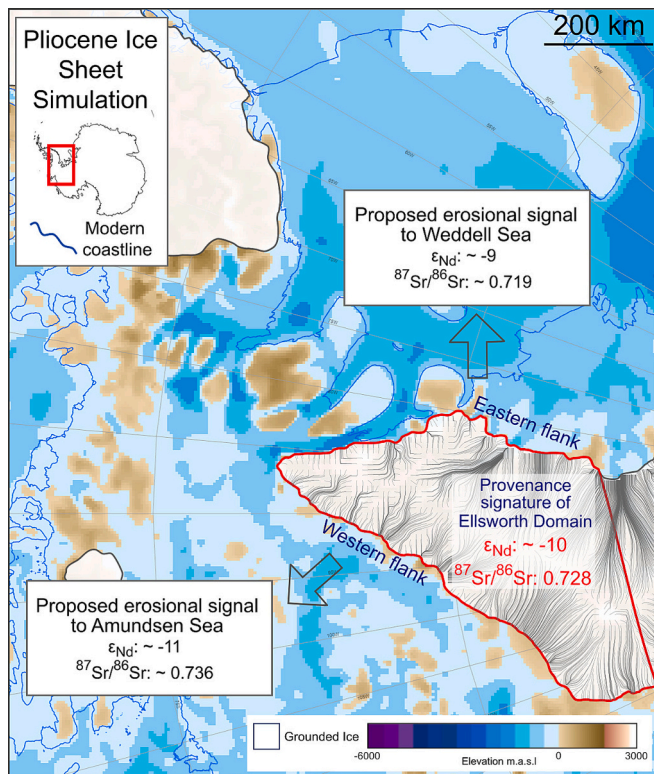


Fig. 10. Estimated provenance signature of detritus supplied from the Ellsworth domain of the EWM crustal block to the Weddell Sea and Amundsen Sea embayments during times of total WAIS collapse. Pliocene ice-sheet model derived ice extent (application of marine ice sheet instability only) (DeConto et al., 2021) and simulated ice flow lines, overlying reconstructed Pliocene median topography (Paxman et al., 2019). Ice flow lines only shown for the EWM block area.

However, the very slow ice flow velocities in the upper Pine Island Glacier catchments suggest low erosion rates and therefore transport of detritus from the Amundsen Sea Embayment at present is likely insignificant (Rignot et al., 2022a; Rignot et al., 2022b). We argue that instead the EWM block signature is currently likely to be restricted to the Weddell Sea. This hypothesis is supported by the relatively radiogenic ϵ_{Nd} values measured in Amundsen Sea Embayment surface sediments beyond the terminus of Pine Island Glacier, alongside detrital hornblende and biotite $^{40}Ar/^{39}Ar$ data dominated by ~ 170 Ma and ~ 270 Ma age peaks (Simões Pereira et al., 2018; Simões Pereira et al., 2020; Marschalek, 2022; Jordan et al., 2025). This is compatible with a primary sediment source from the more proximal Marie Byrd Land, Thurston Island, and Hudson Mountains to the Amundsen Sea.

5.4. Prediction of offshore provenance signatures of a WAIS collapse scenario during past warm periods

Our new provenance characterisation of the EWM crustal block is especially valuable when considering different WAIS extents in the geological past. Ice-sheet model simulations resulting in a fully collapsed WAIS (Sutter et al., 2016; DeConto et al., 2021) indicate that small ice caps remained on highlands (Ross et al., 2014), and outlet glaciers would have calved directly from the EWM into the Weddell Sea and a West Antarctic interior seaway. In such a scenario, EWM detritus could be transported by icebergs and ocean currents to offshore regions other than down present ice flowlines, such as the Bellingshausen, Amundsen and Ross seas.

Major WAIS retreat, at least in the Amundsen Sea sector, might have increased the input of detritus originating from the Ellsworth Mountains, resulting in a shift towards more unradiogenic ϵ_{Nd} values in marine sediments offshore from this sector (Rahaman et al., 2025, Fig. 10). The signature of detritus shed towards the Amundsen Sea Embayment probably differed slightly from that entering the Weddell Sea Embayment due to the heterogeneous spatial distribution of the lithological groups. The EWM contribution towards the Amundsen Sea, excluding the Jurassic granites, is calculated to have had ϵ_{Nd} values of ~ -11 , assuming $>50\%$ of the detritus originated from the Crashsite Group

distributed along the western flank of the EWM (Table S4), along with a zircon U-Pb age spectrum dominated by Ross Orogeny ages (c. 480–590 Ma). In addition, zircon U-Pb ages of ~170 Ma and ~200 Ma representing granitic rocks in the EWM block may also be observed (Craddock et al., 2017b), although Early-Mid Jurassic granitoid magmatism is regionally extensive (Jordan et al., 2025) and therefore not a diagnostic provenance indicator unique to the EWM. Pliocene shifts in ϵ_{Nd} values and Pb isotope data in sediments deposited on the Amundsen Sea continental rise have been attributed to major WAIS retreat towards the EWM during that time (Rahaman et al., 2025; Horikawa et al., 2026). Our data shows the EWM have ϵ_{Nd} values compatible with this hypothesis.

In contrast, EWM detritus transported towards the Weddell Sea Embayment would have been primarily sourced from Upper Heritage Group rocks along the eastern flank of the Ellsworth Mountains (>80%, Table S4), producing estimated ϵ_{Nd} values of ~ -9 and a bimodal distribution of Grenville-aged (c. 1000–1250 Ma) and Ross-aged (c. 480–590 Ma) zircons, similar to those predicted for the modern situation. As in the Amundsen Sea, zircon U-Pb ages of ~170 Ma and ~200 Ma from Jurassic granitic rocks may also be observed (Craddock et al., 2017b).

Our new characterisation of Ellsworth-Whitmore bedrock provides a valuable tool for substantive provenance tracing in sediment cores from around West Antarctica.

6. Conclusions

The different stratigraphic units of the Ellsworth Mountains have distinct geochemical characteristics. This provides a framework and tool for tracing their provenance in marine sediments and constraining WAIS evolution through time. The lowermost Heritage Group members are distinguishable through their dominant Grenville zircon U-Pb ages and ϵ_{Nd} values of ~ -8. The overlying Crashesite Group and Whiteout Conglomerate both show dominant Ross Orogeny age peaks in zircon U-Pb dates but have markedly different Nd isotope compositions (~ -12 and ~ -18, respectively). The signature of the youngest Polarstar Formation is characterised by zircon U-Pb ages of 270 Ma and the most radiogenic ϵ_{Nd} values (~ -4).

Correlating the geology of nunataks located to the SSW of the Ellsworth Mountains to these lithological units substantially increases our knowledge of the geology of the Subglacial Ellsworth Highlands, a region previously uncharacterised from a provenance perspective. Based on their radiogenic isotope and zircon U-Pb age signatures, we conclude that the nunataks are best correlated to either the upper Heritage Group or Crashesite Group of the Ellsworth Mountains with the associated provenance signature.

Modern ice drainage and surface velocity maps indicate that Ellsworth Mountains detritus is presently transported towards the Weddell Sea Embayment via the Rutford and Institute ice streams, with only minor amounts of EWM detritus being supplied by the Pine Island Glacier to the Amundsen Sea Embayment. However, under a WAIS collapse scenario, opening of Trans-Antarctic seaways in West Antarctica may have created pathways to the Amundsen and Ross Sea embayments, which could have allowed the delivery of EWM derived detritus by iceberg rafting and/or ocean current transport into these sectors. Such a scenario was recently suggested on the basis of new provenance data from Early-Middle Pliocene sediments deposited on the Amundsen Sea continental rise (Rahaman et al., 2025; Passchier et al., 2025; Horikawa et al., 2026). We here provide the detailed provenance “fingerprints” for detritus shed from the different stratigraphic units and regions of the EWM crustal block, to substantiate, ground-truth and refine reconstructions of past WAIS retreat based on the provenance signatures observed in marine sedimentary records from around West Antarctica.

CRedit authorship contribution statement

Emily J. Archibald: Writing – original draft, Visualization, Investigation, Formal analysis, Data curation, Conceptualization. **James W. Marschalek:** Writing – review & editing, Supervision, Methodology, Conceptualization. **Adrian R. Muxworthy:** Writing – review & editing, Supervision, Resources, Methodology, Funding acquisition, Conceptualization. **Teal R. Riley:** Writing – review & editing, Resources. **Claus-Dieter Hillenbrand:** Writing – review & editing. **Tom A. Jordan:** Writing – review & editing. **Pieter Vermeesch:** Writing – review & editing, Resources, Formal analysis. **Michael J. Flowerdew:** Writing – review & editing, Resources, Investigation. **Martin Siegert:** Writing – review & editing, Conceptualization. **Dominic A. Hodgson:** Writing – review & editing. **Tina van de Fliedrt:** Writing – review & editing, Supervision, Resources, Project administration, Methodology, Funding acquisition, Conceptualization.

Declaration of competing interest

The authors declare that they have no known competing financial interests or personal relationships that could have appeared to influence the work reported in this paper.

Acknowledgements

E.J.A. thanks the Janet Watson PhD studentship, Department of Earth Science and Engineering, Imperial College London, for financial support for this project. E.J.A. also thanks Katharina Kreissig and Barry Coles for technical assistance in the MAGIC laboratory at Imperial College London; Irena Nevjestic for technical assistance in the SPIN laboratory, Imperial College London; Mark Evans for help with sample collection and preparation at the British Antarctic Survey; and Mark Stanley for technical support with U-Pb zircon dating at University College London.

T.v.d.F. and J.W.M. acknowledge UKRI NERC grants NE/W000172/1 and NE/X009394/1, and A.R.M. acknowledges UKRI NERC grant NE/Z000068/1. Additional funding was provided by the Trans-Antarctic Association grant, which supported SEM work related to this project.

Appendix A. Supplementary data

Supplementary data to this article can be found online at <https://doi.org/10.1016/j.chemgeo.2026.123290>.

Data availability

The data used in this study, including radiogenic isotope values, palaeomagnetic measurements, major oxide composition, and zircon U-Pb data are available in the supplementary material.

References

- Agrios, L.M., Licht, K.J., Williams, T., Hemming, S.R., Welch, L., Micky, J.L., 2021. Detrital geochronology and lithologic signatures of Weddell Sea Embayment ice streams, Antarctica—Implications for subglacial geology and ice sheet history. *Geol. Soc. Am. Bull.* 134, 1895–1915.
- Castillo, P., Fanning, C.M., Fernandez, R., Poblete, F., Hervé, F., 2017. Provenance and age constraints of Paleozoic siliciclastic rocks from the Ellsworth Mountains in West Antarctica, as determined by detrital zircon geochronology. *Geol. Soc. Am. Bull.* 129, 1568–1584.
- Castillo, P., Poblete, F., Fernández, R., Bastías-Silva, J., Fanning, C.M., 2024. Re-evaluating the link between the Ellsworth Mountains and East Antarctica in the Neoproterozoic: implications for the breakup of Rodinia and the existence of Pannotia. *Precambrian Res.* 403.
- Castle, J.W., Craddock, C., 1975. Deposition and metamorphism of polar-star formation (permian), Ellsworth Mountains. *Antarct. J. US* 10, 239–241.
- Church, J., Clark, P., Cazenave, A., GREGORY, J., Jevrejeva, S., Levermann, A., Merrifield, M., Milne, G., Nerem, R., Nunn, P., Payne, A., Pfeffer, W., Stammer, D., Alakkat, U., 2013. *Climate Change 2013: the physical science basis. Contribution of*

- working group I to the fifth assessment report of the intergovernmental panel on climate change. *Sea Level Change* 1138–1191.
- Cox, S.C., Smith Lyttle, B., Elkind, S., Smith Siddoway, C.S., Morin, P., Capponi, G., Abu-Alam, T., Ballinger, M., Bamber, L., Kitchener, B., Lelli, L., Mawson, J.F., Millikin, A., Dal Seno, N., Whitburn, L., White, T., Burton-Johnson, A., Crispini, L., Elliot, D., Elvevold, S., Goodge, J.W., Halpin, J.A., Jacobs, J., Mikhalsky, E., Martin, A.P., Morgan, F., Smellie, J., Scadden, P., Wilson, G.S., 2023. The GeoMAP (v.2022–08) Continent-Wide Detailed Geological Dataset of Antarctica. PANGAEA.
- Craddock, J.P., Fitzgerald, P., Konstantinou, A., Nereson, A., Thomas, R.J., 2017a. Detrital zircon provenance of upper Cambrian-Permian strata and tectonic evolution of the Ellsworth Mountains, West Antarctica. *Gondwana Res.* 45, 191–207.
- Craddock, J.P., Schmitz, M.D., Crowley, J.L., Larocque, J., Pankhurst, R.J., Juda, N., Konstantinou, A., Storey, B., 2017b. Precise U-Pb zircon ages and geochemistry of Jurassic granites, Ellsworth-Whitmore terrane, Central Antarctica. *Geol. Soc. Am. Bull.* 129, 118–136.
- Curtis, M.L., 2001. Tectonic history of the Ellsworth Mountains, West Antarctica: reconciling a Gondwana enigma. *Geol. Soc. Am. Bull.* 113, 939–958.
- Curtis, M., Lomas, S., 1999. Late Cambrian stratigraphy of the Heritage Range, Ellsworth Mountains: implications for basin evolution. *Antarct. Sci.* 11, 63–77.
- Curtis, M.L., Leat, P.T., Riley, T.R., Storey, B.C., Millar, I.L., Randall, D.E., 1999. Middle Cambrian rift-related volcanism in the Ellsworth Mountains, Antarctica: tectonic implications for the palaeo-Pacific margin of Gondwana. *Tectonophysics* 304, 275–299.
- Dalziel, I.W.D., Elliot, D.H., 1982. West Antarctica: problem child of Gondwanaland. *Tectonics* 1, 3–19.
- DeConto, R.M., Pollard, D., Alley, R.B., Velicogna, I., Gasson, E., Gomez, N., Sadai, S., Condon, A., Gilford, D.M., Ashe, E.L., Kopp, R.E., Li, D.W., Dutton, A., 2021. The Paris climate agreement and future sea-level rise from Antarctica. *Nature* 593, 83–89.
- Elliot, D.H., Fanning, C.M., Hulett, S.R.W., 2015. Age provinces in the Antarctic craton: evidence from detrital zircons in Permian strata from the Beardmore Glacier region, Antarctica. *Gondwana Res.* 28, 152–164.
- Favier, L., Durand, G., Cornford, S.L., Gudmundsson, G.H., Gagliardini, O., Gillet-Chaulet, F., Zwinger, T., Payne, A.J., Le Brocq, A.M., 2014. Retreat of Pine Island Glacier controlled by marine ice-sheet instability. *Nat. Clim. Chang.* 4, 117–121.
- Flowerdew, M.J., Millar, I.L., Curtis, M.L., Vaughan, A.P.M., Horstwood, M.S.A., Whitehouse, M.J., Fanning, C.M., 2007. Combined U-Pb geochronology and Hf isotope geochemistry of detrital zircons from early Paleozoic sedimentary rocks, Ellsworth-Whitmore Mountains block, Antarctica. *Geol. Soc. Am. Bull.* 119, 275–288.
- Garrett, S.W., Herrod, L.D.B., Mantripp, D.R., 1987. Crustal structure of the area around Haag Nunataks, West Antarctica: new aeromagnetic and bedrock elevation data. *Gondwana Res.* 4, 109–115.
- Golledge, N.R., Clark, P.U., He, F., Dutton, A., Turney, C.S.M., Fogwill, C.J., Naish, T.R., Levy, R.H., McKay, R.M., Lowry, D.P., Bertler, N.A.N., Dunbar, G.B., Carlson, A.E., 2021. Retreat of the Antarctic Ice Sheet during the last interglaciation and implications for future change. *Geophys. Res. Lett.* 48 e2021GL094513.
- Griffin, W., Powell, W., Pearson, N.J., O'Reilly, S., 2008. GLITTER: Data Reduction Software for Laser Ablation ICP-MS. 40. Laser Ablation-ICP-MS in the earth sciences, pp. 204–207. Mineralogical Association of Canada short course series.
- Hillenbrand, C.-D., Smith, J.A., Hodell, D.A., Greaves, M., Poole, C.R., Kender, S., Williams, M., Andersen, T.J., Jernas, P.E., Elderfield, H., Klages, J.P., Roberts, S.J., Gohl, K., Larter, R.D., Kuhn, G., 2017. West Antarctic ice sheet retreat driven by Holocene warm water incursions. *Nature* 547, 43–48.
- Horikawa, K., Iwai, M., Hillenbrand, C.-D., Siddoway, C.S., Halberstadt, A.R., Cowan, E. A., Penkrot, M.L., Gohl, K., Wellner, J.S., Asahara, Y., Shin, K.-C., Noda, M., Fujimoto, M., Party, E.S., Gohl, K., Wellner, J.S., Klaus, A., Kulhanek, D., Bauersachs, T., Bohaty, S.M., Courtillot, M., Cowan, E.A., de Lira Mota, M.A., Esteves, M.S.R., Fegyveresi, J.M., Frederichs, T., Gao, L., Halberstadt, A.R., Hillenbrand, C.-D., Iwai, M., Kim, J.-H., King, T.M., Klages, J.P., Passchier, S., Penkrot, M.L., Prebble, J.G., Rahaman, W., Reinardy, B.T.I., Renaudie, J., Robinson, D.E., Scherer, R.P., Siddoway, C.S., Wu, L., Yamane, M., 2026. Repeated major inland retreat of Thwaites and Pine Island glaciers (West Antarctica) during the Pliocene. *Proc. Natl. Acad. Sci.* 123 e2508341122.
- Jackson, S.E., Pearson, N.J., Griffin, W.L., Belousova, E.A., 2004. The application of laser ablation-inductively coupled plasma-mass spectrometry to in situ U-Pb zircon geochronology. *Chem. Geol.* 211, 47–69.
- Jacobsen, S.B., Wasserburg, G.J., 1980. Sm-Nd isotopic evolution of chondrites. *Earth Planet. Sci. Lett.* 50, 139–155.
- Jordan, T.A., Ferraccioli, F., Ross, N., Corr, H.F.J., Leat, P.T., Bingham, R.G., Rippin, D. M., Le Brocq, A., Siegert, M.J., 2013. Inland extent of the Weddell Sea Rift imaged by new aerogeophysical data. *Tectonophysics* 585, 137–160.
- Jordan, T.A., Riley, T.R., Siddoway, C.S., 2020. The geological history and evolution of West Antarctica. *Nat. Rev. Earth Environ.* 1, 117–133.
- Jordan, T.A., Johnson, J.S., Riley, T.R., Conrad, E., Carter, A., 2025. Subglacial geology and palaeo flow of Pine Island Glacier from combining glacial erratics with geophysics. *Commun. Earth Environ.* 6, 826.
- Joughin, I., Smith, B.E., Medley, B., 2014. Marine ice sheet collapse potentially under way for the Thwaites Glacier Basin, West Antarctica. *Science* 344, 735–738.
- King, E.C., 2009. Flow dynamics of the Rutford Ice Stream ice-drainage basin, West Antarctica, from radar stratigraphy. *Ann. Glaciol.* 50, 42–48.
- Lau, S.C.Y., Wilson, N.G., Golledge, N.R., Naish, T.R., Watts, P.C., Silva, C.N.S., Cooke, I. R., Allcock, A.L., Mark, F.C., Linse, K., Strugnell, J.M., 2023. Genomic evidence for West Antarctic Ice Sheet collapse during the last Interglacial. *Science* 382, 1384–1389.
- Licht, K.J., Hemming, S.R., 2017. Analysis of Antarctic glacial sediment provenance through geochemical and petrologic applications. *Quat. Sci. Rev.* 164, 1–24.
- Lipp, A.G., Shorttle, O., Syvret, F., Roberts, G.G., 2020. Major element composition of sediments in terms of weathering and provenance: implications for crustal recycling. *Geochem. Geophys. Geosyst.* 21.
- Marschalek, J.W., 2022. Sediment Provenance Constraints on West Antarctic Ice Sheet History. PhD Thesis. Imperial College London.
- Marschalek, J.W., Zurli, L., Talarico, F., Van De Fliedert, T., Vermeesch, P., Carter, A., Beny, F., Bout-Roumazelles, V., Sangiorgi, F., Hemming, S.R., Perez, L.F., Colleoni, F., Prebble, J.G., Van Peer, T.E., Perotti, M., Shevenell, A.E., Browne, I., Kulhanek, D.K., Levy, R., Harwood, D., Sullivan, N.B., Meyers, S.R., Griffith, E.M., Hillenbrand, C.D., Gasson, E., Siegert, M.J., Keisling, B., Licht, K.J., Kuhn, G., Dodd, J.P., Boshuis, C., de Santis, L., McKay, R.M., Expedition, I., 2021. A large West Antarctic ice sheet explains early Neogene Sea-level amplitude. *Nature* 600, 450–455.
- Matsuoka, K., Skoglund, A., Roth, G., DE Pomereu, J., Griffiths, H., Headland, R., Herried, B., Katsumata, K., Le Brocq, A., Licht, K., Morgan, F., Neff, P., Ritz, C., Scheinert, M., Tamura, T., Van de Putte, A., Van Den Broeke, M., Von Deschanden, A., Deschamps-Berger, C., Van Lieferinge, B., Tronstad, S., Melvær, Y., INSTITUTE, N. P., 2018. Quantarctica. Norwegian Polar Institute.
- Morlighem, M., Rignot, E., Binder, T., Blankenship, D., Drews, R., Eagles, G., Eisen, O., Ferraccioli, F., Forsberg, R., Fretwell, P., Goel, V., Greenbaum, J.S., Gudmundsson, H., Guo, J.X., Helm, V., Hofstede, C., Howat, I., Humbert, A., Jokat, W., Karlsson, N.B., Lee, W.S., Matsuoka, K., Millar, R., Mougnot, J., Paden, J., Pattyn, F., Roberts, J., Rosier, S., Ruppel, A., Seroussi, H., Smith, E.C., Steinhage, D., Sun, B., Van Den Broeke, M.R., Van Ommen, T.D., Van Wessem, M., Young, D.A., 2020. Deep glacial troughs and stabilizing ridges unveiled beneath the margins of the Antarctic ice sheet. *Nat. Geosci.* 13, 132–137.
- Pankhurst, R.J., Millar, I.L., Grunow, A.M., Storey, B.C., 1993. The Pre-Cenozoic magmatic history of the Thurston Island Crustal Block, West Antarctica. *J. Geophys. Res. Solid Earth* 98, 11835–11849.
- Passchier, S., Hillenbrand, C.-D., Hemming, S., Ehrmann, W., Frederichs, T., Bohaty, S. M., Leon, R., Libman-Roshal, O., MINO-Moreira, L., Gohl, K., Wellner, J., 2025. West Antarctic ice retreat and paleoceanography in the Amundsen Sea in the warm early Pliocene. *Nat. Commun.* 16, 5609.
- Paxman, G.J.G., Jamieson, S.S.R., Hochmuth, K., Gohl, K., Bentley, M.J., Leitchenkov, G., Ferraccioli, F., 2019. Reconstructions of Antarctic topography since the Eocene-Oligocene boundary. *Palaeogeogr. Palaeoclimatol. Palaeoecol.* 535, 109346.
- Pierce, E.L., Williams, T., Van De Fliedert, T., Hemming, S.R., Goldstein, S.L., Brachfeld, S. A., 2011. Characterizing the sediment provenance of East Antarctica's weak underbelly: the Aurora and Wilkes sub-glacial basins. *Paleoceanography* 26.
- Pinard, P., Protheroe, A., Holland, J., Burgess, S., Statham, P., 2020. Development and validation of standardless and standards-based X-ray microanalysis. *IOP Conf. Ser.: Mater. Sci. Eng.* 891, 012020.
- Pritchard, H.D., Fretwell, P.T., Fremant, A.C., Bodart, J.A., Kirkham, J.D., Aitken, A., Bamber, J., Bell, R., Bianchi, C., Bingham, R.G., Blankenship, D.D., Casassa, G., Christianson, K., Conway, H., Corr, H.F.J., Cui, X., Damaske, D., Damm, V., Dorschel, B., Drews, R., Eagles, G., Eisen, O., Eisermann, H., Ferraccioli, F., Field, E., Forsberg, R., Franke, S., Goel, V., Gogineni, S.P., Greenbaum, J., Hills, B., Hindmarsh, R.C.A., Hoffman, A.O., Holschuh, N., Holt, J.W., Humbert, A., Jacobel, R.W., Jansen, D., Jenkins, A., Jokat, W., Jong, L., Jordan, T.A., King, E.C., Kohler, J., Krabill, W., Maton, J., Gillespie, M.K., Langley, K., Lee, J., Leitchenkov, G., Leuschen, C., Luyendyk, B., Macgregor, J.A., Mackie, E., Moholdt, G., Matsuoka, K., Morlighem, M., Mougnot, J., Nitsche, F.O., Nost, O.A., Paden, J., Pattyn, F., Popov, S., Rignot, E., Rippin, D.M., Rivera, A., Roberts, J.L., Ross, N., Ruppel, A., Schroeder, D.M., Siegert, M.J., Smith, A.M., Steinhage, D., Studinger, M., Sun, B., Tabacco, I., Tinto, K.J., Urbini, S., Vaughan, D.G., Wilson, D. S., Young, D.A., Zirizzotti, A., 2025. Bedmap3 updated ice bed, surface and thickness gridded datasets for Antarctica. *Sci. Data* 12, 414.
- Rahaman, W., Gutjahr, M., Prabhakar, P., 2025. Late Pliocene growth of the West Antarctic Ice Sheet to near-modern configuration. *Nat. Commun.* 16, 6705.
- Randall, D.E., Mac Niocaill, C., 2004. Cambrian palaeomagnetic data confirm a Natal Embayment location for the Ellsworth-Whitmore Mountains, Antarctica, in Gondwana reconstructions. *Geophys. J. Int.* 157, 105–116.
- Randall, D.E., Curtis, M.L., Millar, I.L., 2000. A new late middle Cambrian palaeomagnetic pole for the Ellsworth Mountains, Antarctica. *J. Geol.* 108, 403–425.
- Rignot, E., Mougnot, J., Scheuchl, B., Van Den Broeke, M., Van Wessem, M.J., Morlighem, M., 2019. Four decades of Antarctic ice sheet mass balance from 1979–2017. *Proc. Natl. Acad. Sci.* 116, 1095–1103.
- Rignot, E., Mougnot, J., Scheuchl, B., Jeong, S., 2022a. Changes in Antarctic ice sheet motion derived from satellite radar interferometry between 1995 and 2022. *Geophys. Res. Lett.* 49 e2022GL100141.
- Rignot, E., Scheuchl, B., Mougnot, J., Jeong, S., 2022b. MEASURES Multi-Year Reference Velocity Maps of the Antarctic Ice Sheet, Version 1. NASA National Snow and Ice Data Center Distributed Active Archive Center.
- Riley, T.R., Flowerdew, M.J., Pankhurst, R.J., Millar, I.L., Whitehouse, M.J., 2020a. U-pb zircon geochronology from Haag Nunataks, Coats Land and Shackleton Range (Antarctica): constraining the extent of juvenile Late Mesoproterozoic arc terranes. *Precambrian Res.* 340.
- Riley, T.R., Jordan, T.A., Leat, P.T., Curtis, M.L., Millar, I.L., 2020b. Magmatism of the Weddell Sea rift system in Antarctica: implications for the age and mechanism of rifting and early stage Gondwana breakup. *Gondwana Res.* 79, 185–196.
- Riley, T.R., Carter, A., Hunter, M.A., Millar, I.L., Flowerdew, M.J., Curtis, M.L., Hodgson, D.A., 2025. Provenance and correlation of Permian successions from the Falkland/Malvinas Islands with West Gondwana: implications for a Natal Embayment palaeo-location. *J. Geol. Soc. Lond.* 182 jgs2024-282.

- Ross, N., Bingham, R.G., Corr, H.F.J., Ferraccioli, F., Jordan, T.A., Le Brocq, A., Rippin, D.M., Young, D., Blankenship, D.D., Siegert, M.J., 2012. Steep reverse bed slope at the grounding line of the Weddell Sea sector in West Antarctica. *Nat. Geosci.* 5, 393–396.
- Ross, N., Jordan, T.A., Bingham, R.G., Corr, H.F.J., Ferraccioli, F., Le Brocq, A., Rippin, D.M., Wright, A.P., Siegert, M.J., 2014. The Ellsworth subglacial highlands: inception and retreat of the West Antarctic ice sheet. *Geol. Soc. Am. Bull.* 126, 3–15.
- Roy, M., Van de Fliedert, T., Hemming, S.R., Goldstein, S.L., 2007. ⁴⁰Ar/³⁹Ar ages of hornblende grains and bulk Sm/Nd isotopes of circum-Antarctic glacio-marine sediments: implications for sediment provenance in the southern ocean. *Chem. Geol.* 244, 507–519.
- Shepherd, A., Ivins, E., Rignot, E., Smith, B., Van Den Broeke, M., Velicogna, I., Whitehouse, P., Briggs, K., Joughin, I., Krinner, G., Nowicki, S., Payne, T., Scambos, T., Schlegel, N., A. G., Agosta, C., Ahlström, A., Babonis, G., Barletta, V., Blazquez, A., Bonin, J., Csatho, B., Cullather, R., Felikson, D., Fettweis, X., Forsberg, R., Gallee, H., Gardner, A., Gilbert, L., Groh, A., Gunter, B., Hanna, E., Harig, C., Helm, V., Horvath, A., Horwath, M., Khan, S., Kjeldsen, K.K., Konrad, H., Langen, P., Lecavalier, B., Loomis, B., Luthcke, S., Mcmillan, M., Melini, D., Mernild, S., Mohajerani, Y., Moore, P., Mougnot, J., Moyano, G., Muir, A., Nagler, T., Niell, G., Nilsson, J., Noel, B., Ootaka, I., Pattie, M.E., Peltier, W.R., Pie, N., Rietbroek, R., Rott, H., Sandberg-Sørensen, L., Sasgen, I., Save, H., Scheuchl, B., Schrama, E., Schröder, L., Seo, K.-W., Simonsen, S., Slater, T., Spada, G., Sutterley, T., Talpe, M., Tarasov, L., Van de Berg, W.J., Van Der Wal, W., Van Wessem, M., Vishwakarma, B.D., Wiese, D., Wouters, B., The, I. T., 2018. Mass balance of the Antarctic ice sheet from 1992 to 2017. *Nature* 558, 219–222.
- Simões Pereira, P., Van De Fliedert, T., Hemming, S.R., Hammond, S.J., Kuhn, G., Brachfeld, S., Doherty, C., Hillenbrand, C.-D., 2018. Geochemical fingerprints of glacially eroded bedrock from West Antarctica: detrital thermochronology, radiogenic isotope systematics and trace element geochemistry in late Holocene glacial-marine sediments. *Earth-Sci. Rev.* 182, 204–232.
- Simões Pereira, P., Van De Fliedert, T., Hemming, S.R., Frederichs, T., Hammond, S.J., Brachfeld, S., Doherty, C., Kuhn, G., Smith, J.A., Klages, J.P., Hillenbrand, C.-D., 2020. The geochemical and mineralogical fingerprint of West Antarctica's weak underbelly: Pine Island and Thwaites glaciers. *Chem. Geol.* 550.
- Sláma, J., Košler, J., Condon, D.J., Crowley, J.L., Gerdes, A., Hanchar, J.M., Horstwood, M.S.A., Morris, G.A., Nasdala, L., Norberg, N., Schaltegger, U., Schoene, B., Tubrett, M.N., Whitehouse, M.J., 2008. Plešovice zircon — a new natural reference material for U–Pb and Hf isotopic microanalysis. *Chem. Geol.* 249, 1–35.
- Small, D., Bentley, M.J., Freeman, S.P.H.T., Rodés, A., Xu, S., 2025. A pre-Pliocene origin of the glacial trimline in the Ellsworth mountains and the prevalence of old landscapes at high elevations in West Antarctica. *Geomorphology* 473, 109634.
- Smith, B., Fricker, H.A., Gardner, A.S., Medley, B., Nilsson, J., Paolo, F.S., Holschuh, N., Adusumilli, S., Brunt, K., Csatho, B., Harbeck, K., Markus, T., Neumann, T., Siegfried, M.R., Zwally, H.J., 2020. Pervasive ice sheet mass loss reflects competing ocean and atmosphere processes. *Science* 368, 1239–1242.
- Storey, B.C., Macdonald, D.I.M., 1987. Sedimentary-rocks of the Ellsworth-Thiel mountains ridge and their regional equivalents. *Br. Antarct. Surv. Bull.* 21–49.
- Storey, B.C., Dalziel, I.W.D., Garrett, S.W., Grunow, A.M., Pankhurst, R.J., Vennum, W. R., 1988. West Antarctica in Gondwanaland: crustal blocks, reconstruction and breakup processes. *Tectonophysics* 155, 381–390.
- Storey, B.C., Pankhurst, R.J., Johnson, A.C., 1994. The Grenville province within Antarctica - A test of the sweat hypothesis. *J. Geol. Soc. Lond.* 151, 1–4.
- Sutter, J., Gierz, P., Grosfeld, K., Thoma, M., Lohmann, G., 2016. Ocean temperature thresholds for last Interglacial West Antarctic Ice Sheet collapse. *Geophys. Res. Lett.* 43, 2675–2682.
- Tanaka, T., Togashi, S., Kamioka, H., Amakawa, H., Kagami, H., Hamamoto, T., Yuhara, M., Orihashi, Y., Yoneda, S., Shimizu, H., Kunimaru, T., Takahashi, K., Yanagi, T., Nakano, T., Fujimaki, H., Shinjo, R., Asahara, Y., Tanimizu, M., Dragusanu, C., 2000. JNdi-1: a neodymium isotopic reference in consistency with LaJolla neodymium. *Chem. Geol.* 168, 279–281.
- van den Akker, T., Lipscomb, W.H., Leguy, G.R., Bernales, J., Berends, C.J., van de Berg, W.J., van de Wal, R.S.W., 2025. Present-day mass loss rates are a precursor for West Antarctic Ice Sheet collapse. *Cryosphere* 19, 283–301.
- Vermeesch, P., 2013. Multi-sample comparison of detrital age distributions. *Chem. Geol.* 341, 140–146.
- Vermeesch, P., 2018. IsoplotR: a free and open toolbox for geochronology. *Geosci. Front.* 9, 1479–1493.
- Vermeesch, P., 2021a. Maximum depositional age estimation revisited. *Geosci. Front.* 12, 843–850.
- Vermeesch, P., 2021b. On the treatment of discordant detrital zircon U–Pb data. *Geochronology* 3, 247–257.
- Watts, D.R., Bramall, A.M., 1981. Palaeomagnetic evidence for a displaced terrain in Western Antarctica. *Nature* 293, 638–640.
- Webers, G.F., Craddock, C., Spletstoesser, J.F., Geological Society of America, 1992. *Geology and Paleontology of the Ellsworth Mountains, West Antarctica*. Geological Society of America, Boulder.
- Weis, D., Kieffer, B., Maerschalk, C., Barling, J., De Jong, J., Williams, G.A., Hanano, D., Pretorius, W., Mattielli, N., Scoates, J.S., Goolaerts, A., Friedman, R.M., Mahoney, J. B., 2006. High-precision isotopic characterization of USGS reference materials by TIMS and MC-ICP-MS. *Geochem. Geophys. Geosyst.* 7 p.n/a.
- Wiedenbeck, M., Hanchar, J.M., Peck, W.H., Sylvester, P., Valley, J., Whitehouse, M., Kronz, A., Morishita, Y., Nasdala, L., Fiebig, J., Franchi, I., Girard, J.-P., Greenwood, R.C., Hinton, R., Kita, N., Mason, P.R.D., Norman, M., Ogasawara, M., Piccoli, P.M., Rhede, D., Satoh, H., Schulz-Dobrick, B., Skår, O., Spicuzza, M., Terada, K., Tindle, A., Togashi, S., Vennemann, T., Xie, Q., Zheng, Y.-F., 2004. Further characterisation of the 91500 zircon crystal. *Geostand. Geoanal. Res.* 28, 9–39.